

The Ronne Ice Shelf survived the last interglacial

<https://doi.org/10.1038/s41586-024-08394-w>

Received: 12 August 2024

Accepted: 8 November 2024

Published online: 29 January 2025

Open access

 Check for updates

Eric W. Wolff^{1✉}, Robert Mulvaney², Mackenzie M. Grieman¹, Helene M. Hoffmann^{1,3}, Jack Humby², Christoph Nehrbass-Ahles^{1,4}, Rachael H. Rhodes¹, Isobel F. Rowell^{1,2}, Louise C. Sime¹, Hubertus Fischer⁵, Thomas F. Stocker⁵, Amaelle Landais⁶, Frédéric Parrenin⁷, Eric J. Steig⁸, Marina Dütsch⁹ & Nicholas R. Golledge¹⁰

The fate of the West Antarctic Ice Sheet (WAIS)¹ is the largest cause of uncertainty in long-term sea-level projections. In the last interglacial (LIG) around 125,000 years ago, data suggest that sea level was several metres higher than today^{2–4}, and required a significant contribution from Antarctic ice loss, with WAIS usually implicated. Antarctica and the Southern Ocean were warmer than today^{5–8}, by amounts comparable to those expected by 2100 under moderate to high future warming scenarios. However, direct evidence about the size of WAIS in the LIG is sparse. Here we use sea salt data from an ice core from Skytrain Ice Rise, adjacent to WAIS, to show that, during most of the LIG, the Ronne Ice Shelf was still in place, and close to its current extent. Water isotope data are consistent with a retreat of WAIS⁹, but seem inconsistent with more dramatic model realizations¹⁰ in which both WAIS and the large Antarctic ice shelves were lost. This new constraint calls for a reappraisal of other elements of the LIG sea-level budget. It also weakens the observational basis that motivated model simulations projecting the highest end of projections for future rates of sea-level rise to 2300 and beyond.

The West Antarctic Ice Sheet (WAIS) is considered particularly vulnerable to retreat due to climate change¹¹, primarily because it is mainly marine-based, sitting on a bed below sea level. The reverse bed slope (deepening inland) beneath the margins of much of WAIS makes it potentially subject to irreversible retreat due to marine ice sheet instability (MISI)^{12–14}. The range of projections of future sea-level contributions from Antarctica for a given climate scenario is large¹¹. A number of ice-sheet modelling studies project loss of much of WAIS under the highest warming scenarios (for example, representative concentration pathway RCP 8.5)^{15,16}, but this loss generally occurs over several centuries. By the year 2200 CE, most of these models predict only a few tens of centimetres of sea-level rise from Antarctica (particularly WAIS), even under RCP 8.5 (refs. 15–17). However, one model, which applied a large ocean warming, and which includes the extra proposed mechanisms of hydrofracturing and marine ice cliff instability (MICI)¹⁸, predicts much faster and greater loss of ice from WAIS and other parts of Antarctica, reaching the equivalent of 5 m of sea-level rise by 2200^{10,19}.

The model configuration and ocean forcing of these studies^{10,19} were partly motivated by consideration of possible ice loss during the last interglacial (LIG, about 130–115 thousand years ago (ka)). Both Greenland²⁰ and Antarctica^{6,7} were warmer during the LIG than at present. Synthesis of relative sea-level data, derived mainly from corals and interpreted using glacial isostatic modelling, has suggested that global mean sea level during the LIG may have been 6–9 m higher than today^{2,11}.

After taking account of a contribution of up to 1 m from thermosteric expansion of seawater²¹ and mountain glaciers, a large contribution from the Greenland and Antarctic ice sheets is required to reach this higher sea level. Most studies estimate at most a 2-m LIG sea-level input from the Greenland Ice Sheet^{22–24}, which suggests a substantial Antarctic sea-level contribution. One study estimates²⁵ a greater contribution from Greenland of 5.1 m, but because this study constrains peak input to late in the LIG (about 121 ka), it still requires a substantial Antarctic input at 125 ka. More recent studies estimating a LIG global eustatic sea-level rise of 1.2–5.3 m above present³ or even 0.4–2.7 m above present⁴ reduce the requirement for Antarctic ice loss. Nonetheless, most studies have inferred from the sea-level and Greenland data that the size of the Antarctic Ice Sheet (and probably WAIS) must have been substantially reduced in the LIG²⁶.

Only a few ice-sheet modelling studies have tried to predict the state of the Antarctic Ice Sheet during the LIG, and their estimates of ice loss from Antarctica range from zero in the absence of significant ocean warming²⁷, up to 7.5 m of sea-level equivalent¹⁰. The study that included the MICI mechanism¹⁰ produced a LIG Antarctic ice loss of greater than 6 m sea-level equivalent, including complete loss of the Ronne–Filchner and Ross ice shelves. Other work^{9,28} suggested a more modest loss of ice in the WAIS region, with up to 3 m (ref. 28) or 4 m (ref. 9) of sea-level equivalent compared to today. In these studies, loss was focussed in the Amundsen Sea region, and the Ronne Ice Shelf was retained at close to its present configuration.

¹Department of Earth Sciences, University of Cambridge, Cambridge, UK. ²British Antarctic Survey, Cambridge, UK. ³Geo- and Environmental Center, University of Tübingen, Tübingen, Germany. ⁴National Physical Laboratory, Teddington, UK. ⁵Climate and Environmental Physics, Physics Institute, and Oeschger Centre for Climate Change, University of Bern, Bern, Switzerland. ⁶Laboratoire des Sciences du Climat et de l'Environnement, LSCE/IPSL, CEA-CNRS-UVSQ, Université Paris-Saclay, Gif-sur-Yvette, France. ⁷Université Grenoble Alpes, CNRS, INRAE, IRD, Grenoble INP, IGE, Grenoble, France. ⁸Department of Earth and Space Sciences and Department of Atmospheric Sciences, University of Washington, Seattle, WA, USA. ⁹Department of Meteorology and Geophysics, University of Vienna, Vienna, Austria. ¹⁰Antarctic Research Centre, Victoria University of Wellington, Wellington, New Zealand. ✉e-mail: ew428@cam.ac.uk

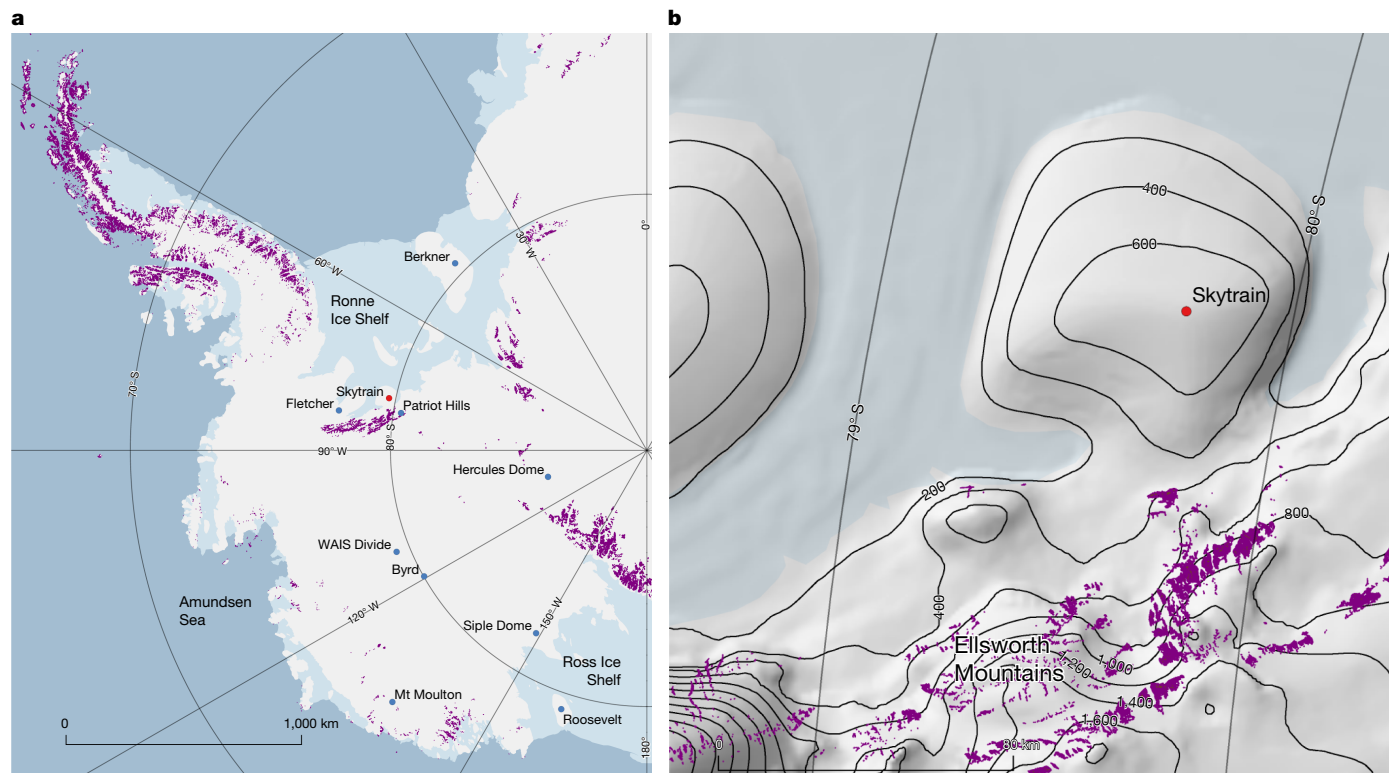


Fig. 1 | The location of the SIR drilling site. SIR is shown as a red dot and other existing and proposed ice core sites around WAIS as blue dots. The purple colour shows exposed rock outcrops. **a**, Overview of West Antarctica. **b**, Detail

of the SIR region. Contours are from the Cryosat2 elevation model⁴². Maps in **a** and **b** were generated using QGIS with the Quantarctica mapping environment⁴³, under a Creative Commons licence CC BY 4.0.

Direct proximal evidence of the state of WAIS during the LIG has so far been missing. However, a recent paper²⁹ studying the genomics of an octopus species around the Antarctic continent suggests that seaways may have existed between the Ronne, Amundsen and Ross embayments, with a timing which is inferred to represent the LIG. This would imply a substantial loss of ice in the LIG.

The only published LIG ice core record from WAIS is a horizontal ice trench record from Mount Moulton (Fig. 1)³⁰. An early interpretation of the differences in the LIG water isotope data between Mount Moulton and East Antarctic sites, using isotope-enabled climate model output, led to a tentative qualitative interpretation that WAIS did collapse in the LIG³¹. However, a more comprehensive recent modelling study³² did not support this conclusion, and instead suggested that the Mount Moulton isotope record is rather insensitive to WAIS collapse. A horizontal ice trench record from blue ice in the Patriot Hills (Fig. 1)³³ suggested a LIG hiatus in ice deposition or preservation that was initially interpreted as supporting substantial LIG mass loss in the Weddell Sea embayment. However, subsequent work has suggested a different interpretation involving changes in ice flow induced by bedrock uplift and more modest local thinning⁹.

Here we present data from the Skytrain Ice Rise (SIR) ice core, which provides proxy-based estimates of ice shelf extent, local ice elevation and, in combination with data from other cores and studies, constraints on the extent of WAIS ice loss in the LIG.

Skytrain Ice Rise

SIR is an ice cap, independent from the main body of WAIS, that sits at the landward margin of the Ronne Ice Shelf adjacent to WAIS (Fig. 1). SIR is expected to have remained an independent ice cap throughout the last glacial cycle because it is separated from the main ice sheet by the high barrier of the Ellsworth Mountains and it has bedrock sitting

above sea level surrounded radially almost entirely by bathymetry greater than 1,000 m.

An ice core was drilled to bedrock at SIR (651 m depth)³⁴, and was subsequently dated, giving an age model tied to those of other Antarctic ice cores³⁵. Although there is evidence of flow disturbance in the lowest 50 m of the ice (beyond 108 ka), ice from 117–126 ka (617–627 m) in the LIG is present and is in stratigraphic order³⁵ (Methods). Unfortunately, ice from the very warmest part of the LIG between 127 and 129 ka is missing from our record, even though older ice is present below the LIG section³⁵.

SIR sea salt record

Sodium (Na) is used as a sea salt indicator in the ice core record. Sea salt is transported and deposited to ice sheets from the saline surfaces of sea ice and the open ocean. Its concentration in ice cores is therefore influenced by the pattern and strength of atmospheric transport and by sea ice extent³⁶. To reach SIR, sea salt must travel from the ice front across the non-marine Ronne Ice Shelf, whose front is now 680 km from the drill site. As a result, a first-order control on sea salt concentration at SIR is distance from the source (the ice shelf edge) to SIR. A spatial survey along the Ronne Ice Shelf³⁷ shows a rapid decrease in sea salt concentration with distance inland from the ice shelf front, demonstrating the predominant influence of the Weddell Sea on sea salt deposition across the ice shelf. If the ice shelf disintegrated, bringing salty surfaces closer to SIR, we would expect much higher than present Na concentration.

In fact, we find that Na concentration across the warm plateau of the LIG from 126 to 117 ka was lower than today, reaching late Holocene concentrations only late in the LIG, at 120 ka (Fig. 2, Extended Data Table 1 and Extended Data Fig. 1). Although we cannot rule out some effects from changing transport and/or sea ice, this low Na concentration suggests that the ice shelf could actually have been extended beyond its current position at 126 ka, as it was in the early Holocene³⁷. It then retreated to

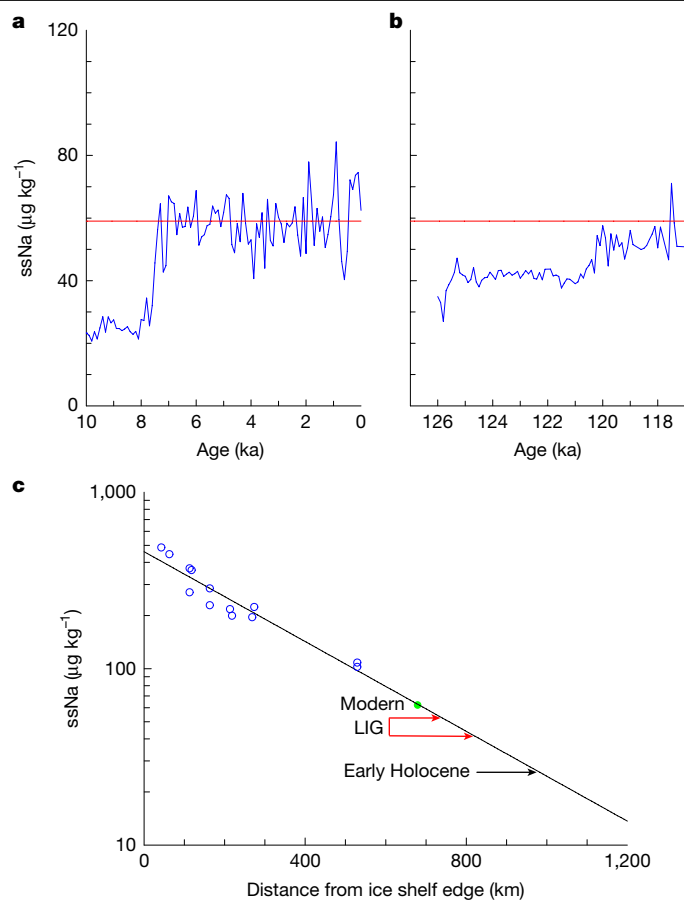


Fig. 2 | Sea salt sodium (ssNa) concentration at SIR comparing the Holocene and LIG. **a**, Holocene (10–0 ka, 100 year averages). **b**, LIG (126–117 ka, 100 year averages). The red line in **a** and **b** is the average value for 7–0 ka. **c**, Data from a published spatial survey (blue circles) of sea salt concentrations on the Ronne Ice Shelf³⁷. The solid black line is the best fit³⁸ and the green circle is the present concentration at SIR (top 25 m of core) which fits closely onto the line. The vertical position of the black arrow is the average ssNa concentrations from 10–8 ka, when the Ronne Ice Shelf was extended. The red arrows labelled LIG indicate average ssNa values from 125–121 ka (lower arrow) and 120–118 ka (upper arrow).

near its current position at about 120 ka. This would be consistent with what occurred in the Holocene, when the ice shelf edge was extended beyond its current position in the early Holocene, and retreated to its current position only at 7.3 ka (ref. 38). There is no sign of the concentrations of around 400 $\mu\text{g kg}^{-1}$ that the spatial survey shown in Fig. 2 suggests would be expected if the ice shelf disintegrated completely.

SIR water isotope record

Like sea salt, the water isotope signal at SIR in the LIG results from a combination of environmental changes. The differences between LIG and Holocene values will be a response to three components: (1) change in climate (temperature and sea ice); (2) local elevation change at SIR and (3) change in large-scale circulation resulting from changes in the morphology of Antarctica, here potentially the loss of WAIS. If components (1) and (2) can be estimated then we can adjust the measured data to provide component (3), which is diagnostic of large-scale changes in the WAIS. Recent modelling work³² found that if WAIS was almost completely lost in the LIG³⁹, $\delta^{18}\text{O}$ at SIR would increase by about 4‰ compared to present, after accounting for a local change in elevation and assuming a modern climate.

The expected Antarctic spatial pattern of $\delta^{18}\text{O}$ due to LIG climate (component (1)) can be estimated from model simulations, in which

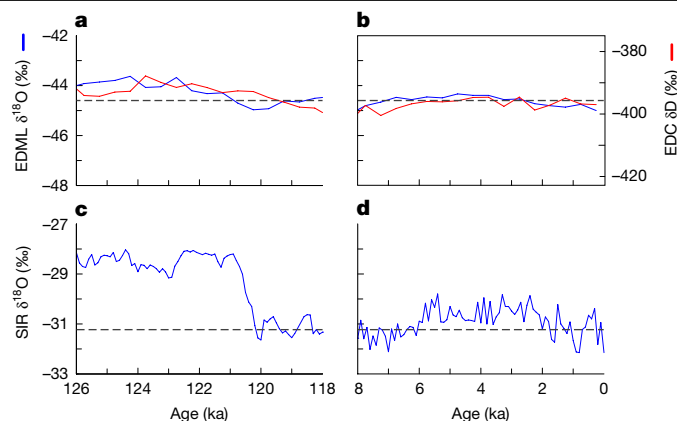


Fig. 3 | $\delta^{18}\text{O}$ for the SIR ice and East Antarctic cores in the LIG and Holocene. **a**, Reference data for the LIG for EPICA Dome C (EDC)⁶ (red, δD) and EPICA Dronning Maud Land (EDML)⁴⁴ (blue, $\delta^{18}\text{O}$), scaled 8:1, with the horizontal line being an indicative level for the late Holocene. **b**, As **a** but for the last 8 kyr. **c**, SIR data for the LIG. **d**, SIR data for the last 8 kyr. The dashed line in **c** and **d** is the average of 2–0 ka. All three records are synchronized to the AICC2012 age model. The y-scaling is the same for all three cores and both time periods.

orbital and greenhouse gas values are changed from pre-industrial values to those of the LIG and all other parameters are kept constant. Such model simulations produce only a small net change in isotopic values⁴⁰ but with spatial variability of about 1‰ across the continent. This is consistent with measured $\delta^{18}\text{O}$ values for 120–126 ka at five East Antarctic reference sites, which show an average increase of +0.7‰ (range 0.3–1.3‰) relative to those of the last 7.5 kyr (Fig. 3, Extended Data Fig. 2 and Extended Data Table 2), although this may also contain an element due to elevation change³². By contrast, the $\delta^{18}\text{O}$ value at SIR between 126 and 120 ka is much larger: +2.5‰ above the late Holocene (2–0 ka) value (or +2.2‰ above that of the last 7.5 ka). This suggests that, after removing the signal arising from continent-wide changes in climate, the net isotopic signal at SIR due to changes in site elevation and large-scale changes in circulation is probably between about 1 and 2‰.

To constrain component (2) (site elevation) we consider total air content (TAC) of the ice. SIR TAC (without cut-bubble correction; Methods) for the LIG (average of 126–120 ka) was $125.3 \pm 0.6 \text{ ml kg}^{-1}$ (mean \pm s.e.m.), which is higher than the late Holocene (2–0.45 ka) value of $121.1 \pm 0.7 \text{ ml kg}^{-1}$ (Extended Data Fig. 3). Adjusting for the different cut-bubble correction in the two time periods caused by the reduction in bubble size under pressure deeper in the ice sheet (Methods) and accounting for the temperature change estimated from the measured change in $\delta^{18}\text{O}$ (Methods), we estimate that the elevation at Skytrain in the LIG was either $150 \pm 90 \text{ m}$ lower (if the pore volume V_c was invariant between the two periods) or $60 \pm 80 \text{ m}$ lower (if pore volume varied with temperature). With an estimated $\delta^{18}\text{O}$ -elevation gradient of $0.8 \pm 0.2\%$ per 100 m (Methods), local changes in altitude could account for up to 2‰ of the 2.5‰ change in $\delta^{18}\text{O}$ at SIR between the LIG and the Holocene.

Combining these estimates of components (1) and (2) suggests that component (3), from changes in circulation resulting from large-scale changes to the topography of the WAIS, is between 0 and 2‰. Although this value is uncertain, it is at most about half that predicted by the high-resolution isotope model³² for the case of a near-complete WAIS collapse. Nonetheless, the water isotope values at SIR in the LIG are significantly higher than those in the Holocene, which certainly indicates loss of ice, either at SIR itself (elevation effect) or across WAIS more generally, and probably both.

WAIS, Ronne Ice Shelf and the LIG

Our Na results indicate that the Ronne Ice Shelf was intact between 126 and 120 ka, and may have been more extensive than today in the

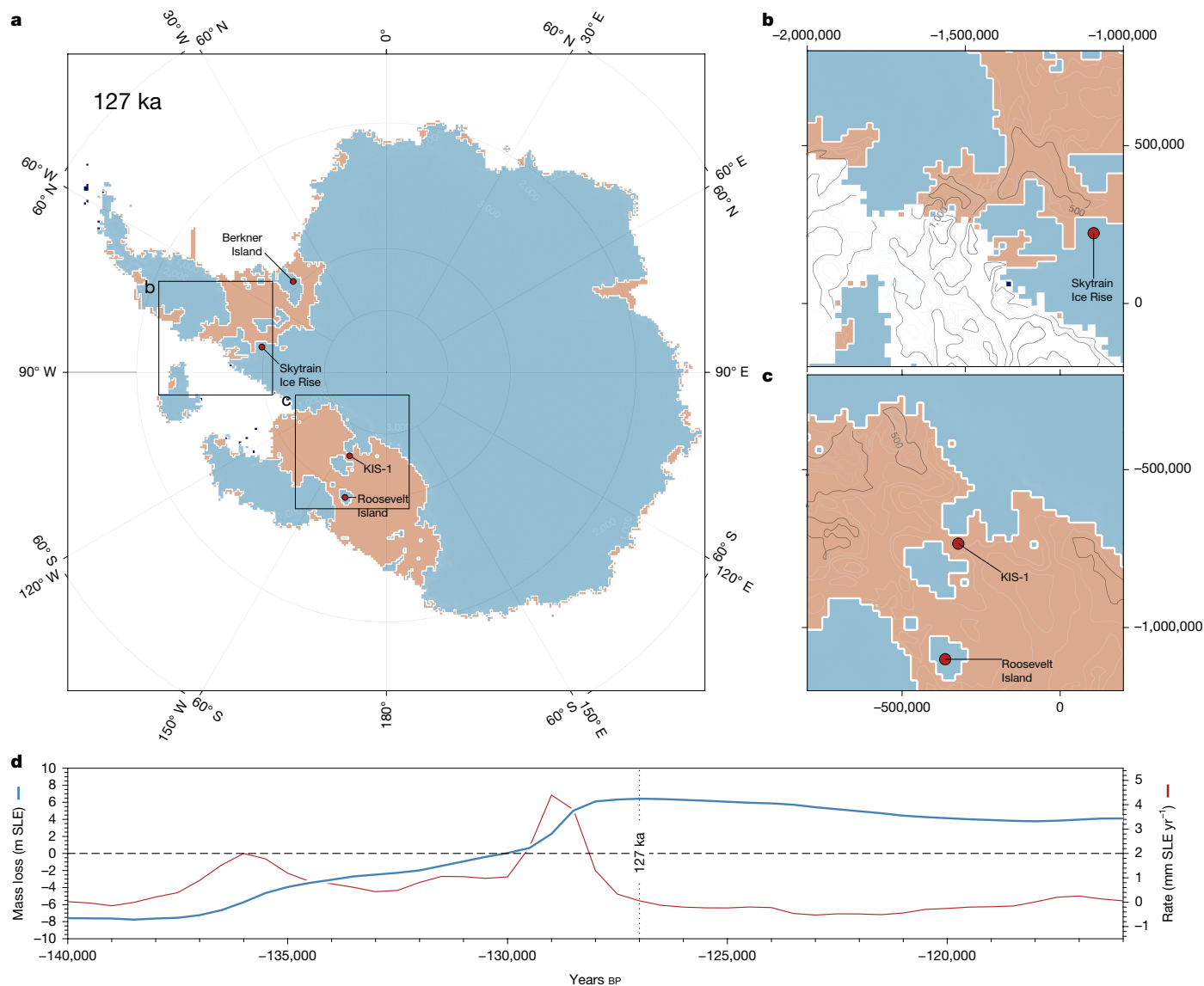


Fig. 4 | A model reconstruction of the Antarctic Ice Sheet at the LIG. The model is consistent with both our data showing the presence of ice shelves (absence of exposed ocean or sea ice) and data indicating the existence of seaways. **a–c**, Antarctica (**a**); close-up of region around SIR (**b**); close-up of region in Ross Ice Shelf (**c**). In **a–c**, blue is grounded ice, pink is ice shelf.

b and **c** show water column thickness contours, with units of metres, for the ocean beneath the ice shelves. **d**, Time series of modelled magnitude (blue) and rate (red) of sea-level-equivalent mass loss for the shown scenario. Model output maps were plotted using Generic Mapping Tools v.6.

early part of that period. Although we have no data for the period of maximum Antarctic warmth between 130 and 126 ka, it is unlikely that the ice shelf disappeared and then regrew under the warm, low sea ice, conditions of this period. Probabilistic sea-level reconstructions suggest that the LIG sea-level maximum occurred at or after 126 ka (ref. 41), arguing against substantial ice growth before then. Furthermore, model simulations show that, despite increasing mass loss from the continent during this interval, the extent of the Ronne Ice Shelf remained largely unchanged (Extended Data Fig. 4). We therefore conclude that the Ronne Ice Shelf survived the LIG, with a minimum extent similar to or greater than that of the present.

A recent study suggested that LIG seaways accounted for observed gene transfer between the Weddell, Amundsen and Ross Sea sectors of Antarctica in a species of deep-living octopus²⁹. These two sets of results are not mutually exclusive, but can be reconciled with an Antarctic configuration in which ice in the Amundsen Sea sector was significantly reduced, but the ice shelves, fed by ice streams in the Ross and Ronne catchments, were intact. This also implies that the inferred seaways

existed at depth but were covered by ice shelf and did not represent a source of open water, sea ice or sea salt aerosol. Figure 4 illustrates a possible ice sheet/shelf configuration that reconciles our new data from SIR with that from the octopus study²⁹. The simulation shown is derived from a previously published ensemble⁹. In this scenario, loss of WAIS occurs as a consequence of ocean thermal driving in the Amundsen Sea embayment that triggers marine ice sheet instability. However, CCSM3-simulated cooler-than-present ocean temperatures in the Ross and Weddell Seas facilitate ice shelf preservation in these larger two embayments. The result is an ice geometry in which Na flux to SIR from the Weddell Sea is low throughout the interglacial (Methods).

The net water isotopic signal at SIR between 126 and 120 ka (compared to the Holocene) is less (perhaps half) than that predicted for complete loss of WAIS³². In the absence of isotope-enabled climate model simulations at high resolution involving a partial collapse, or of robust results from other models with enough resolution to diagnose the response at SIR, we conclude that our results are consistent with a partial (but not full) collapse of WAIS, focussed on the Amundsen Sea sector. We again can

draw no direct conclusions for the period 130–126 ka, but we suggest that regrowth of WAIS under such warm conditions is unlikely to have occurred.

Our findings are compatible with ice-sheet model simulations in which retreat occurred mainly in the Amundsen Sea sector⁹, but they are not consistent with simulations in which ocean warming and MICI led to great loss of ice in the Weddell (and Ross) Sea sectors¹⁰. This has some important consequences. First, if the main centre of ice loss was the Amundsen Sea sector, with continued ice shelf buttressing of ice flowing into the Ronne and Ross ice shelves, then the magnitude and rate of LIG sea-level rise above present as a result of Antarctic ice loss are probably well below those proposed in ref. 10. Although estimates of LIG sea-level contributions from Antarctica in simulations that retain the large ice shelves vary across ensembles of model realizations (for example, Fig. 4), values of 4 m (ref. 9) are cited, and lower values still could be expected if not all the Amundsen Sea sector ice was lost, as our small isotopic change might suggest. This is sufficient to explain more modest recent estimates of LIG sea-level rise^{3,4}, but cannot be reconciled with the larger values used in many reviews and earlier studies^{1,2,26} unless Greenland contributed earlier than expected or there was a significant contribution from East Antarctica. A second conclusion is that our finding that the Ronne Ice Shelf survived the LIG weakens the observational basis to support projections of the most extreme WAIS loss by 2200, as suggested by simulations involving significant LIG sub-ice shelf ocean warming and the MICI mechanism^{10,19}. Finally, our results refine the recent evidence from octopus DNA²⁹ suggesting that WAIS was significantly reduced in size during a part of the LIG which was only modestly warmer than today. They do, however, pose a challenge to understand how long a period of seaway opening is sufficient to lead to the genomic findings, and whether there are mechanisms that can explain how the genetic material is transported under several hundred kilometres of covered ice shelf. Further ice cores reaching the LIG, such as that planned for Hercules Dome, along with high-resolution modelling of a range of possible WAIS configurations, will be crucial to advance our use of the LIG to constrain future Antarctic ice loss.

Online content

Any methods, additional references, Nature Portfolio reporting summaries, source data, extended data, supplementary information, acknowledgements, peer review information; details of author contributions and competing interests; and statements of data and code availability are available at <https://doi.org/10.1038/s41586-024-08394-w>.

1. IPCC. *Special Report on the Ocean and Cryosphere in a Changing Climate* (eds Pörtner, H.-O. et al.) (Cambridge Univ. Press, 2019).
2. Dutton, A. et al. Sea-level rise due to polar ice-sheet mass loss during past warm periods. *Science* **349**, aaa4019 (2015).
3. Dyer, B. et al. Sea-level trends across The Bahamas constrain peak last interglacial ice melt. *Proc. Natl Acad. Sci. USA* **118**, e2026839118 (2021).
4. Dumitru, O. A. et al. Last interglacial global mean sea level from high-precision U-series ages of Bahamian fossil coral reefs. *Quat. Sci. Rev.* **318**, 108287 (2023).
5. Capron, E. et al. Temporal and spatial structure of multi-millennial temperature changes at high latitudes during the Last Interglacial. *Quat. Sci. Rev.* **103**, 116–133 (2014).
6. Jouzel, J. et al. Orbital and millennial Antarctic climate variability over the last 800,000 years. *Science* **317**, 793–796 (2007).
7. Sime, L. C., Wolff, E. W., Oliver, K. I. C. & Tindall, J. C. Evidence for warmer interglacials in East Antarctic ice cores. *Nature* **462**, 342–345 (2009).
8. Chadwick, M., Sime, L. C., Allen, C. S. & Guarino, M. V. Model-data comparison of Antarctic winter sea-ice extent and Southern Ocean sea-surface temperatures during marine isotope stage 5e. *Paleoceanogr. Paleoclimatol.* **38**, e2022PA004600 (2023).
9. Golledge, N. R. et al. Retreat of the Antarctic ice sheet during the Last Interglaciation and implications for future change. *Geophys. Res. Lett.* **48**, e2021GL094513 (2021).
10. DeConto, R. M. & Pollard, D. Contribution of Antarctica to past and future sea-level rise. *Nature* **531**, 591–597 (2016).
11. Oppenheimer, M. et al. in *IPCC Special Report on the Ocean and Cryosphere in a Changing Climate* (eds Pörtner, H.-O. et al.) 321–445 (Cambridge Univ. Press, 2019).
12. Weertman, J. Stability of the junction between an ice sheet and an ice shelf. *J. Glaciol.* **13**, 3–11 (1974).
13. Mercer, J. H. West Antarctic ice sheet and CO₂ greenhouse effect—threat of disaster. *Nature* **271**, 321–325 (1978).

14. Pattyn, F. & Morlighem, M. The uncertain future of the Antarctic ice sheet. *Science* **367**, 1331–1335 (2020).
15. Bulthuis, K., Arnst, M., Sun, S. & Pattyn, F. Uncertainty quantification of the multi-centennial response of the Antarctic ice sheet to climate change. *Cryosphere* **13**, 1349–1380 (2019).
16. Golledge, N. R. et al. The multi-millennial Antarctic commitment to future sea-level rise. *Nature* **526**, 421 (2015).
17. Ritz, C. et al. Potential sea-level rise from Antarctic ice-sheet instability constrained by observations. *Nature* **528**, 115–118 (2015).
18. Pollard, D., DeConto, R. M. & Alley, R. B. Potential Antarctic ice sheet retreat driven by hydrofracturing and ice cliff failure. *Earth Planet. Sci. Lett.* **412**, 112–121 (2015).
19. DeConto, R. M. et al. The Paris Climate Agreement and future sea-level rise from Antarctica. *Nature* **593**, 83–89 (2021).
20. NEEM Community Members. Eemian interglacial reconstructed from a Greenland folded ice core. *Nature* **493**, 489–494 (2013).
21. Shackleton, S. et al. Global ocean heat content in the Last Interglacial. *Nat. Geosci.* **13**, 77–81 (2020).
22. Goelzer, H., Huybrechts, P., Loutre, M. F. & Fichefet, T. Last Interglacial climate and sea-level evolution from a coupled ice sheet–climate model. *Clim. Past* **12**, 2195–2213 (2016).
23. Helsen, M. M., van de Berg, W. J., van de Wal, R. S. W., van den Broeke, M. R. & Oerlemans, J. Coupled regional climate–ice-sheet simulation shows limited Greenland ice loss during the Eemian. *Clim. Past* **9**, 1773–1788 (2013).
24. Quiquet, A., Ritz, C., Punge, H. J. & Salas y Mélia, D. Greenland ice sheet contribution to sea level rise during the last interglacial period: a modelling study driven and constrained by ice core data. *Clim. Past* **9**, 353–366 (2013).
25. Yau, A. M., Bender, M. L., Robinson, A. & Brook, E. J. Reconstructing the last interglacial at Summit, Greenland: insights from GISP2. *Proc. Natl Acad. Sci. USA* **113**, 9710–9715 (2016).
26. Barnett, R. L. et al. Constraining the contribution of the Antarctic Ice Sheet to Last Interglacial sea level. *Sci. Adv.* **9**, eadf0198 (2023).
27. Sutter, J., Gierz, P., Grosfeld, K., Thoma, M. & Lohmann, G. Ocean temperature thresholds for Last Interglacial West Antarctic Ice Sheet collapse. *Geophys. Res. Lett.* **43**, 2675–2682 (2016).
28. Clark, P. U. et al. Oceanic forcing of penultimate deglacial and last interglacial sea-level rise. *Nature* **577**, 660–664 (2020).
29. Lau, S. C. Y. et al. Genomic evidence for West Antarctic Ice Sheet collapse during the Last Interglacial. *Science* **382**, 1384–1389 (2023).
30. Korotkikh, E. V. et al. The last interglacial as represented in the glaciochemical record from Mount Moulton Blue Ice Area, West Antarctica. *Quat. Sci. Rev.* **30**, 1940–1947 (2011).
31. Steig, E. J. et al. Influence of West Antarctic Ice Sheet collapse on Antarctic surface climate. *Geophys. Res. Lett.* **42**, 4862–4868 (2015).
32. Dütsch, M., Steig, E. J., Blossey, P. N. & Pauling, A. G. Response of water isotopes in precipitation to a collapse of the West Antarctic Ice Sheet in high-resolution simulations with the weather research and forecasting model. *J. Clim.* **36**, 5417–5430 (2023).
33. Turney, C. S. M. et al. Early Last Interglacial ocean warming drove substantial ice mass loss from Antarctica. *Proc. Natl Acad. Sci. USA* **117**, 3996–4006 (2020).
34. Mulvaney, R. et al. Ice drilling on Skytrain Ice Rise and Sherman Island, Antarctica. *Ann. Glaciol.* **62**, 311–323 (2021).
35. Mulvaney, R. et al. The ST22 chronology for the Skytrain Ice Rise ice core. Part 2: An age model to the last interglacial and disturbed deep stratigraphy. *Clim. Past* **19**, 851–864 (2023).
36. Wolff, E. W., Rhodes, R. H. & Legrand, M. in *Chemistry in the Cryosphere* Vol. 3 (eds Shepson, P. B. & Domine, F.) 365–410 (World Scientific, 2021).
37. Minikin, A., Wagenbach, D., Graf, W. & Kipfstuhl, J. Spatial and seasonal variations of the snow chemistry at the central Filchner–Ronne Ice Shelf, Antarctica. *Ann. Glaciol.* **20**, 283–290 (1994).
38. Grieman, M. M. et al. Abrupt Holocene ice loss due to thinning and ungrounding in the Weddell Sea embayment. *Nat. Geosci.* **17**, 227–232 (2024).
39. Pollard, D. & DeConto, R. M. Modelling West Antarctic ice sheet growth and collapse through the past five million years. *Nature* **458**, 329–U389 (2009).
40. Holloway, M. D. et al. Antarctic last interglacial isotope peak in response to sea ice retreat not ice-sheet collapse. *Nat. Commun.* **7**, 12293 (2016).
41. Kopp, R. E., Simons, F. J., Mitrovica, J. X., Maloof, A. C. & Oppenheimer, M. A probabilistic assessment of sea level variations within the last interglacial stage. *Geophys. J. Int.* **193**, 711–716 (2013).
42. Helm, V., Humbert, A. & Miller, H. Elevation and elevation change of Greenland and Antarctica derived from CryoSat-2. *Cryosphere* **8**, 1539–1559 (2014).
43. Matsuoka, K. et al. Quantarctica, an integrated mapping environment for Antarctica, the Southern Ocean, and sub-Antarctic islands. *Environ. Model. Softw.* **140**, 105015 (2021).
44. EPICA Community Members. One-to-one hemispheric coupling of millennial polar climate variability during the last glacial. *Nature* **444**, 195–198 (2006).

Publisher's note Springer Nature remains neutral with regard to jurisdictional claims in published maps and institutional affiliations.



Open Access This article is licensed under a Creative Commons Attribution 4.0 International License, which permits use, sharing, adaptation, distribution and reproduction in any medium or format, as long as you give appropriate credit to the original author(s) and the source, provide a link to the Creative Commons licence, and indicate if changes were made. The images or other third party material in this article are included in the article's Creative Commons licence, unless indicated otherwise in a credit line to the material. If material is not included in the article's Creative Commons licence and your intended use is not permitted by statutory regulation or exceeds the permitted use, you will need to obtain permission directly from the copyright holder. To view a copy of this licence, visit <http://creativecommons.org/licenses/by/4.0/>.

© The Author(s) 2025

The ice core at SIR was drilled to bedrock at 651 m in the field season 2018–2019³⁴, and analysed using continuous flow analysis (CFA) as well as discrete sampling between 2019 and 2021⁴⁵.

Dating

Beyond the top 2,000 years⁴⁶, the ST22 age scale used here was created using the PaleoChrono inverse model and a range of tie points that fix the age scale to AICC2012 ages³⁵. Tie points came from ice chemistry and ¹⁰Be in the ice and from CH₄ and δ¹⁸O_{atm} in the air. It was established that there is flow disturbance below 605 m (108 ka), and that ice from the early peak of the LIG (126–130 ka) and the penultimate glacial maximum is missing. Nonetheless the combined use of CH₄ and δ¹⁸O_{atm} across the main part of the LIG provides clear evidence that the section from 117 to 126 ka is present and in the correct sequence. Paired CH₄–δ¹⁸O_{atm} values are found that have not occurred anywhere else in the last 200 ka other than in the Holocene and in the LIG around 122 ka (Extended Data Fig. 5). The estimated uncertainty in age during the Holocene reference period is about 100 years. The quoted uncertainty for the LIG is less than 300 years, although it is difficult, given the flow disturbance above and below this section, to be sure that there are not nonlinear age–depth relationships between the CH₄/δ¹⁸O_{atm} measurements, which are 1–2 kyr apart.

We do not know exactly why ice from about 127–140 ka, below the dated LIG section, is missing. Detailed examination of CH₄/δ¹⁸O_{atm} values³⁵ in four data points in the 5 m of ice immediately below the LIG section match reference data with ages 140–180 ka. Looking further up the core, we find no possible matches younger than this until at least 60 ka in three cases. Given that 60 ka ice is 80 m higher up the core in a region with flat radar horizons and no evidence of disturbance, we feel confident in saying that ice of age 140–180 ka is present below our LIG section³⁵, which suggests that ice remained present at SIR throughout the penultimate glacial maximum and LIG, as predicted in all ice modelling studies of the LIG that we are aware of. As discussed in more detail elsewhere³⁵, we conclude that flow disturbance caused by interaction between ice of different rheologies is responsible for the missing ice.

Analyses

Na and Ca were measured using ICP-MS and CFA⁴⁵. The ssNa was calculated by correcting for the terrestrial component,

$$\text{ssNa} = \frac{R_t[\text{Na}] - [\text{Ca}]}{R_t - R_m} \quad (1)$$

where R_t and R_m are the weight ratio of Ca to Na in average crust and in seawater (1.78 and 0.038), respectively^{38,47}. The average correction for both the Holocene (0–10 ka) and the LIG (120–126 ka) is only 3%. The uncertainty in concentration between the different periods shown is determined by the uncertainty in calibration, which was estimated at 1.6% (ref. 45).

Stable water isotopes (δ¹⁸O and δD) were measured continuously on the CFA meltstream using a Picarro L2130-I cavity ring down spectrometer³⁸. The continuous measurements were compared with those made on discrete samples using a similar instrument but that could be more carefully and regularly calibrated. The discrete samples were taken approximately once every 10 m for the Holocene, whereas, for the LIG, discrete samples were collected throughout at 10 or 20-cm intervals.

Only the discrete samples were used to calculate deuterium excess (d_s = δD – 8δ¹⁸O), which is particularly sensitive to small uncertainties in the calibration of the two isotopes. The 24 deuterium excess values for the last 2 kyr have a mean of 6.1‰ with an s.d. of 1.1‰ (s.e.m. 0.22‰); for 126–120 ka, 33 discrete values have a mean of 4.9‰, with an s.d. of 0.65‰ (s.e.m. 0.11‰).

TAC was measured using discrete samples of approximately 60 g of ice using a wet-extraction method³⁸. Data (not corrected for cut bubbles) are shown in Extended Data Fig. 3. At various depths we used elongated cuboid samples of different dimensions to estimate the cut-bubble correction⁴⁸; plotting measured TAC against the ratio of sample surface area to volume (S/V); the intercept is the corrected TAC for the given depth, whereas the gradient allows for correction of other samples with known S/V (Extended Data Fig. 6). Between 100 and 200 m (approximately 0.45–2 ka), the cut-bubble correction (excluding one outlier) is $6 \pm 1.1\%$ (mean, s.e.m.) for typical 60 g samples with dimensions $28.5 \times 28.5 \times 90 \text{ mm}^3$. The data for ice of different sizes are too scattered at most depths to derive a robust relationship between the cut-bubble correction and depth (Extended Data Fig. 6). If we assume that the LIG and Holocene ice had similar numbers and shapes of bubbles at the lock-in depth, which is estimated at 48 m in both the Holocene and the LIG³⁵, then we expect the cut-bubble correction to reduce as bubbles get smaller with depth (D), so that fewer of them intersect the edge of the sample, as $D^{-1/3}$. This then implies that, to compare data from the LIG (about 600 m) with the late Holocene (100–200 m), we need to adjust LIG data by $-2.8 \pm 0.7\%$. We apply this adjustment to LIG data in the calculations of elevation that follow, but we refrain from correcting individual TAC values at this stage to avoid introducing assumptions about bubble number and shape for intermediate depths, including the last glacial maximum.

Estimating how much isotopic change is due to elevation change

The pressure at the time and depth of close-off (closely related to atmospheric pressure) is given by:

$$P_c = \left(\frac{\text{TAC}}{V_c} \right) \times \left(\frac{T_c}{T_s} \right) \times P_s \quad (2)$$

where TAC is the total air content after correction for cut bubbles, V_c and T_c are the pore volume per unit mass and temperature at close-off, and T_s and P_s normalize the data to standard temperature and pressure. T_c is calculated using the difference in δ¹⁸O between the LIG and early Holocene, and an isotopic lapse rate of $0.8 \pm 0.2\%$ per 100 m, which was estimated³⁸ on the basis of earlier data and model studies^{49,50}. Early work⁵¹ suggested that V_c increases with site temperature, at least spatially, with a relationship derived for warmer sites such as Skytrain of $V_c = 4.5 \times 10^{-4} \times T + 0.02$, where V_c is in ml kg⁻¹ and T is temperature (K). However, it is not clear if this applies temporally. Site elevation for Antarctica can be estimated as $-7588 \times \ln(P_c/989.1)$ (ref. 52), so that the difference in elevation between two time periods (1 and 2) is

$$\Delta_{\text{elev}} = -7,588 \times \ln \left(\frac{P_{c1}}{P_{c2}} \right) \quad (3)$$

We then use TAC and δ¹⁸O in two sections in which TAC is relatively constant with depth (126–120 ka and 2–0.45 ka) along with the LIG cut-bubble adjustment described above and the δ¹⁸O/ T gradient to estimate the elevation change using equations (2) and (3). We used a Monte Carlo calculation to propagate the uncertainties in the values of TAC at the two time periods, the cut-bubble adjustment and the δ¹⁸O/ T gradient for two different cases, one in which V_c changes with T according to the spatial gradient and one in which it is invariant with temperature.

The small change in elevation between the LIG and Holocene is used in the text to estimate how much of the observed LIG–Holocene change in δ¹⁸O results from a lapse rate change in temperature. We used the same isotopic lapse rate as above.

Water isotope modelling

Estimates of the expected change in water isotopes across Antarctica owing to the atmospheric circulation changes associated with

a reduced or collapsed WAIS are taken from a paper³² that used the high-resolution Weather Research and Forecasting model with the addition of water isotope physics. For its main case, an Antarctic Ice Sheet (AIS) orography was used³⁹ in which WAIS experienced total collapse. The Ronne and Ross ice shelf elevations were reduced to sea level although they remained ice-covered. The change in $\delta^{18}\text{O}$ at SIR centred on 4.5‰, making it a particularly sensitive site to WAIS loss. As SIR in the provided orography was reduced in elevation by about 50 m, the elevation-corrected change in $\delta^{18}\text{O}$ can be estimated for this model run as 4‰. A related modelling study (but with a lower resolution model and without isotopes) found that the atmospheric circulation response and associated surface temperature (and, by inference, water isotope) signal is linear as a function of elevation change⁵³. This supports our inference that the ice loss for the real WAIS might have been only about half as much as for the 'full collapse' scenario. Finally, the high-resolution simulations³² indicate a reduction in deuterium excess ($\text{dex} = \delta\text{D} - 8\delta^{18}\text{O}$) at SIR of about 1‰ with full collapse. Deuterium excess at SIR is 1.2‰ lower in the LIG (126–120 ka) than in the late Holocene (2–0 ka), using only our well-calibrated discrete samples, further supporting the interpretation that the SIR data do indicate some WAIS loss.

Estimating ice shelf extent

To estimate the extent of the Ronne Ice Shelf, we followed the same procedure as in a recent study of the Holocene at SIR³⁸. A thorough study of the concentration of sea salt ions with distance from the ice shelf edge on the Ronne Ice Shelf³⁷ allows us (after converting their chloride values to the equivalent ssNa concentration using sea salt ratios) to derive a strong linear relationship of $\ln[\text{ssNa}]$ versus distance from the ice shelf edge (Fig. 2). This relationship is represented by the equation, $[\text{ssNa}] = 460 \times \exp(-0.0029x)$, where x is distance from the edge of the ice shelf in kilometres. The present-day ssNa concentration of SIR falls very close to the best fit line. We then plot (Fig. 2) the concentrations for different times in the LIG to estimate the changing distance from the ice edge and therefore changing extents of the ice shelf.

Although distance from the source is a first-order control on sea salt, we acknowledge that sea ice extent, atmospheric lifetime and wind strength/direction play second-order roles and could alter the slope of the best fit line we show in Fig. 2c. This would somewhat alter the estimates of ice shelf extent we give, but such effects cannot plausibly negate the factor 10 increase in sea salt we would have expected if the ice shelf had disappeared.

In making these estimates, we assume that any change in elevation has a minimal effect on Na concentration compared to the effect of source distance. This is supported by previous work³⁴ from shallow ice cores, which found no change in Na concentration across a 900-m gradient in elevation around Berkner Island. At SIR, sea salt did not significantly change during an early Holocene isotopic event which was interpreted as being a 400 m elevation change³⁸.

We note that ice sheet model simulations in which ice from the Amundsen Sea sector of Antarctica is removed could place open water closer to SIR in that direction (for example, Fig. 4). However the existence of the Ellsworth Mountains and a remnant high elevation ice sheet around it would restrict transport from that direction. Additionally, atmospheric models indicate that the removal of WAIS ice tends to strengthen surface winds on the Ronne Ice Shelf from the Weddell Sea direction³². If some salt does reach SIR from the Amundsen Sea direction in the LIG this would further lower the contribution from the Weddell Sea, requiring an even more distant ice shelf edge than we have estimated.

Ice sheet modelling

To assess whether it is possible to retain a Ronne Ice Shelf of a comparable extent to present throughout the LIG, while also allowing for the significant loss of WAIS as suggested by genomic data, we explore

a previously published ensemble of LIG simulations⁹. Those experiments used the parallel ice sheet model (PISM)⁵⁵ to transiently simulate the evolution of the AIS through the penultimate glacial maximum and into the LIG²⁸. Taking environmental boundary conditions from transient CCSM3 ocean–atmosphere simulations for termination 1 as well as termination 2, the PISM experiments explored a range of glaciological and solid-earth parameters to find a combination with which ice sheet advance to last glacial maximum extent and retreat to present-day extent, could be captured. These parameters were then used to investigate how much more ice loss may have occurred during the LIG. It was concluded⁹ that the AIS could have sustained approximately 4 m sea-level-equivalent ice loss (compared to the modelled present-day extent using the same parameters), reaching a maximum at around 126 ka. Yet the LIG ice sheet configuration produced in that experiment was one of partial, not complete, WAIS collapse. Subsequent research shows that open seaways may have existed during the LIG that connected the Weddell, Amundsen and Ross Seas, necessitating more complete WAIS collapse. Here we present a scenario in which those open seaways are captured, while also allowing persistent ice shelves in the Weddell and Ross embayments. However, this scenario is based on a parameterization that uses an unrealistically viscous mantle ($10^{21} \text{ Pa s}^{-1}$). This parameterization does not reflect the much weaker mantle characteristics of WAIS that geophysical studies have shown, nor does it allow for a last glacial maximum-to-present simulation that fits well with observations. Because of these shortcomings, we emphasize that the reconstruction presented in Fig. 4 is not empirically validated. Its value, however, is in its internal glaciological consistency (the physics governing ice flow are robustly captured) and in its ability to demonstrate that such a configuration is physically plausible. No doubt there may be other parameterizations in which a similar ice sheet/shelf pattern could be reproduced while also fitting more closely to the present-day. Full details of model parameterization and simulation methodology are presented in previous papers^{9,28}.

Data availability

The water isotope, Na and TAC data presented in this paper are archived in the Pangaea database^{56–59}. The map in Fig. 1 was generated using QGIS with the Quantarctica mapping environment, under a Creative Commons licence CC BY 4.0. The rock outcrop data in the Quantarctica environment, and shown in Fig. 1 are from ref. 60, European Geosciences Union, under a Creative Commons licence CC BY 3.0. The model output maps in Fig. 4 and Extended Data Fig. 4 were plotted using Generic Mapping Tools v.6.

- Grieman, M. M. et al. Continuous flow analysis methods for sodium, magnesium and calcium detection in the Skytrain ice core. *J. Glaciol.* **68**, 90–100 (2021).
- Hoffmann, H. M. et al. The ST22 chronology for the Skytrain Ice Rise ice core. Part 1: A stratigraphic chronology of the last 2000 years. *Clim. Past* **18**, 1831–1847 (2022).
- Röthlisberger, R. et al. Dust and sea salt variability in central East Antarctica (Dome C) over the last 45 kyrs and its implications for southern high-latitude climate. *Geophys. Res. Lett.* **29**, 1963 (2002).
- Martinerie, P., Lipenkov, V. Y. & Raynaud, D. Correction of air-content measurements in polar ice for the effect of cut bubbles at the surface of the sample. *J. Glaciol.* **36**, 299–303 (1990).
- Werner, M., Jouzel, J., Masson-Delmotte, V. & Lohmann, G. Reconciling glacial Antarctic water stable isotopes with ice sheet topography and the isotopic paleothermometer. *Nat. Commun.* **9**, 3537 (2018).
- Goursaud, S. et al. Antarctic ice sheet elevation impacts on water isotope records during the Last Interglacial. *Geophys. Res. Lett.* **48**, e2020GL091412 (2021).
- Martinerie, P., Raynaud, D., Etheridge, D. M., Barnola, J.-M. & Mazaudier, D. Physical and climatic parameters which influence the air content in polar ice. *Earth Planet. Sci. Lett.* **112**, 1–13 (1992).
- Stone, J. O. Air pressure and cosmogenic isotope production. *J. Geophys. Res. Solid Earth* **105**, 23753–23759 (2000).
- Pauling, A. G., Bitz, C. M. & Steig, E. J. Linearity of the climate system response to raising and lowering West Antarctic and coastal Antarctic topography. *J. Clim.* **36**, 6195–6212 (2023).
- Wagenbach, D. et al. Reconnaissance of chemical and isotopic firn properties on top of Berkner Island, Antarctica. *Ann. Glaciol.* **20**, 307–312 (1994).

55. Winkelmann, R. et al. The Potsdam Parallel Ice Sheet Model (PISM-PIK). Part 1: Model description. *Cryosphere* **5**, 715–726 (2011).
56. Wolff, E. W. et al. Water isotope data for the full Skytrain Ice Rise ice core obtained using the CFA melt stream [dataset]. *Pangaea* <https://doi.org/10.1594/PANGAEA.973226> (2024).
57. Wolff, E. W. et al. Water isotope data for the full Skytrain Ice Rise ice core obtained using discrete samples, and used to calculate deuterium excess [dataset]. *Pangaea* <https://doi.org/10.1594/PANGAEA.973167> (2024).
58. Wolff, E. W. et al. Sodium and calcium data from the full Skytrain Ice Rise ice core [dataset]. *Pangaea* <https://doi.org/10.1594/PANGAEA.973178> (2024).
59. Wolff, E. W., Nehrbass-Ahles, C., King, A. C. F. & Bauska, T. K. Total air content data for the Skytrain Ice Rise ice core [dataset]. *Pangaea* <https://doi.org/10.1594/PANGAEA.973190> (2024).
60. Burton-Johnson, A., Black, M., Fretwell, P. T. & Kaluza-Gilbert, J. An automated methodology for differentiating rock from snow, clouds and sea in Antarctica from Landsat 8 imagery: a new rock outcrop map and are a estimation for the entire Antarctic continent. *Cryosphere* **10**, 1665–1677 (2016).
61. Fischer, H. et al. Reconstruction of millennial changes in transport, dust emission and regional differences in sea ice coverage using the deep EPICA ice cores from the Atlantic and Indian Ocean sector of Antarctica. *Earth Planet. Sci. Lett.* **260**, 340–354 (2007).
62. Petit, J. R. et al. Climate and atmospheric history of the past 420,000 years from the Vostok ice core, Antarctica. *Nature* **399**, 429–436 (1999).
63. Stenni, B. et al. Expression of the bipolar see-saw in Antarctic climate records during the last deglaciation. *Nat. Geosci.* **4**, 46–49 (2011).
64. Kawamura, K. et al. Northern Hemisphere forcing of climatic cycles over the past 360,000 years implied by accurately dated Antarctic ice cores. *Nature* **448**, 912–916 (2007).
65. Steig, E. J. et al. Synchronous climate changes in Antarctica and the North Atlantic. *Science* **282**, 92–95 (1998).

Acknowledgements We thank J. Rix, S. Polfrey, R. Tuckwell, C. McKeever and logistic colleagues at the British Antarctic Survey for their support in drilling the core. We also thank S. Miller, C. Durman, A. King, E. Ludlow, L. Thomas and V. Alcock for help with cutting, processing and analysing the ice core. This project has received funding from the European

Research Council under the Horizon 2020 research and innovation programme (grant agreement no. 742224, WACSWAIN). This material reflects only the authors' views and the Commission is not liable for any use that may be made of the information contained therein. T.F.S. acknowledges funding from the Swiss National Science Foundation (grant nos 172745 and 200492) and all authors from the University of Bern gratefully acknowledge the long-term support of ice core science by the Swiss National Science Foundation. E.W.W. and H.M.H. have also been funded for part of this work through a Royal Society Professorship. N.R.G. acknowledges funding from the Ministry for Business, Innovation and Employment contracts RTVU2206 (Our Changing Coast) and ANTA1801 (Antarctic Science Platform), as well as from the Royal Society of New Zealand, contract MFP-GNS1901. Development of PISM is supported by NASA grants 20-CRYO2020-0052 and 80NSSC22K0274 and NSF grant OAC-2118285. E.J.S. acknowledges funding from the US National Science Foundation (grant nos 1602435, 1841844 and 2045075). For the purpose of open access, the author has applied a Creative Commons Attribution (CC BY) licence to any Author Accepted Manuscript version arising from this submission.

Author contributions E.W.W. conceived the project, based on earlier studies by R.M. R.M., E.W.W., C.N.-A. and M.M.G. drilled and logged the ice core, along with engineering and logistic colleagues. E.W.W., M.M.G., H.M.H., J.H., R.M., C.N.-A. and I.F.R. processed the ice core. M.M.G., H.M.H., J.H., I.F.R., R.H.R. and R.M. carried out the CFA analysis of the core and C.N.-A. measured the TAC. H.F. and T.F.S. provided methane measurements of discrete samples. A.L. provided measurements of $\delta^{18}\text{O}_{\text{atm}}$. R.M., E.W.W. and F.P. led the dating of the deep ice. E.J.S., M.D. and L.C.S. provided interpretation of the isotope modelling and N.R.G. contributed expertise in ice sheet modelling, including the production of Fig. 4. All authors contributed to interpretation of the data. E.W.W. drafted the paper and all authors edited it.

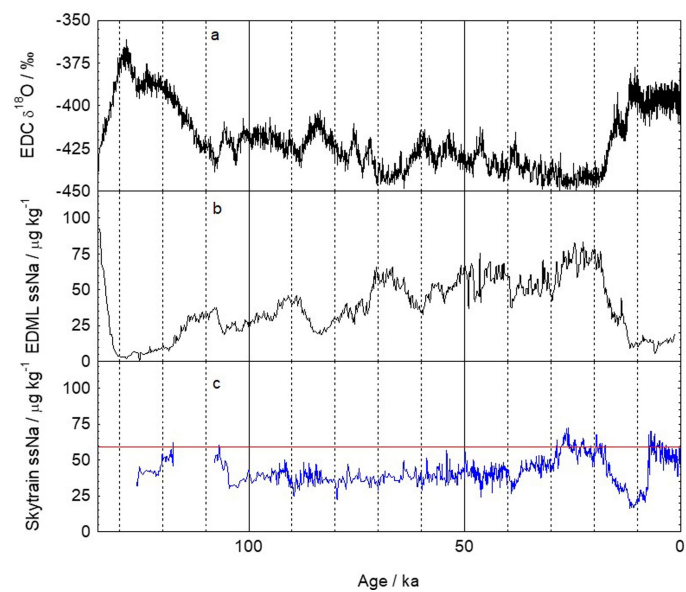
Competing interests The authors declare no competing interests.

Additional information

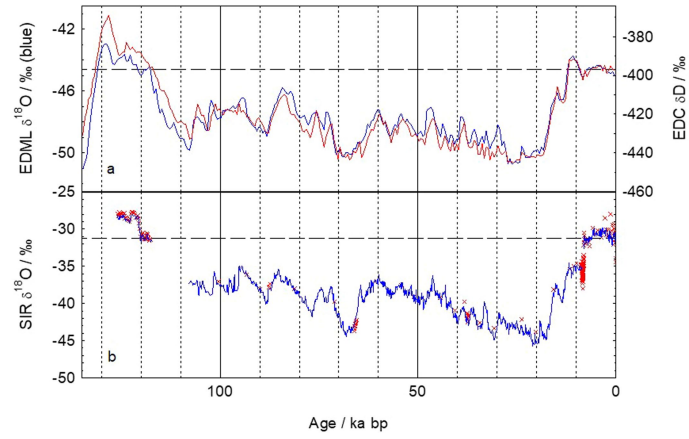
Correspondence and requests for materials should be addressed to Eric W. Wolff.

Peer review information *Nature* thanks Javier Blasco and the other, anonymous, reviewer(s) for their contribution to the peer review of this work.

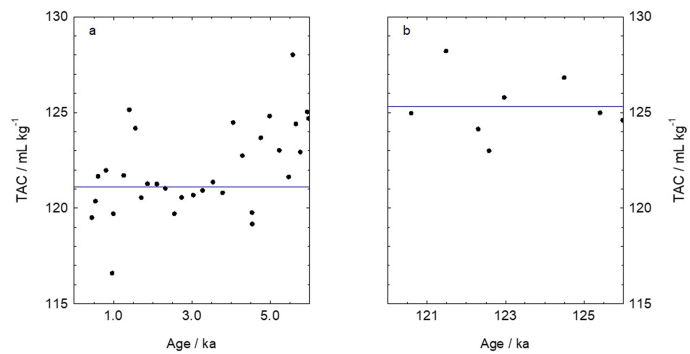
Reprints and permissions information is available at <http://www.nature.com/reprints>.



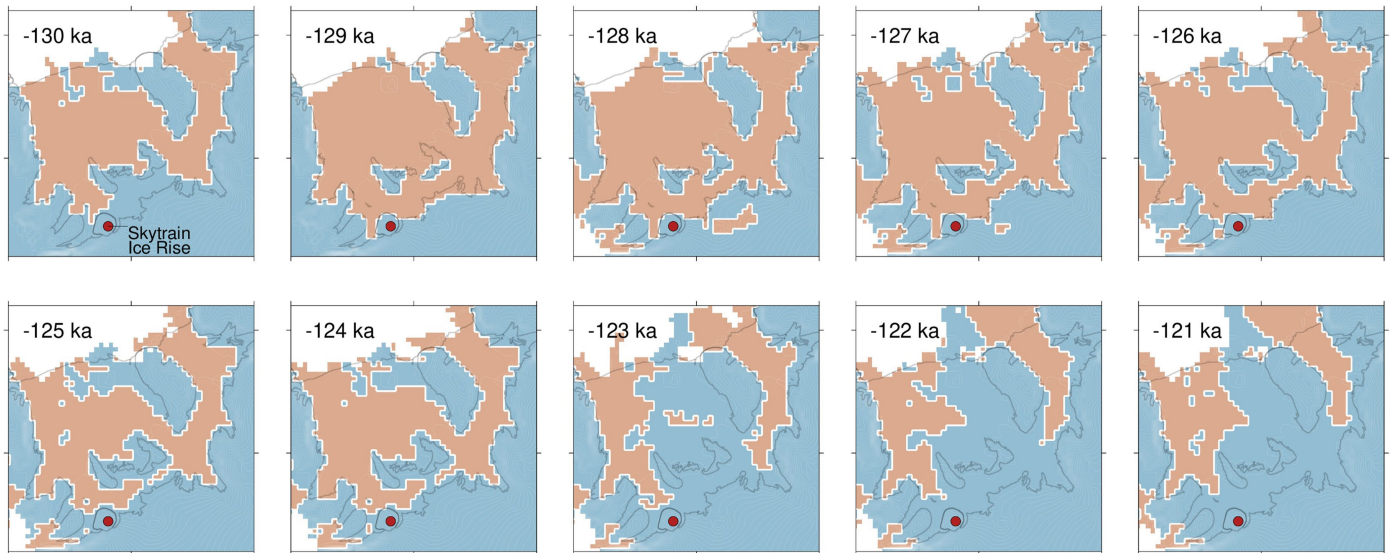
Extended Data Fig. 1 | ssNa data over the last glacial cycle, showing the interglacials in context. (a) Deuterium record of climate at Dome C⁶ to provide context for the progression of climate across Antarctica. (b) ssNa at EDML⁶¹ for comparison with SIR (c) ssNa at SIR (100 year means, dated sections only); a datapoint at 481.0 m where there is a visible ash layer is not plotted. The red line shows the average concentration of ssNa at SIR in the period from 7-5 ka.



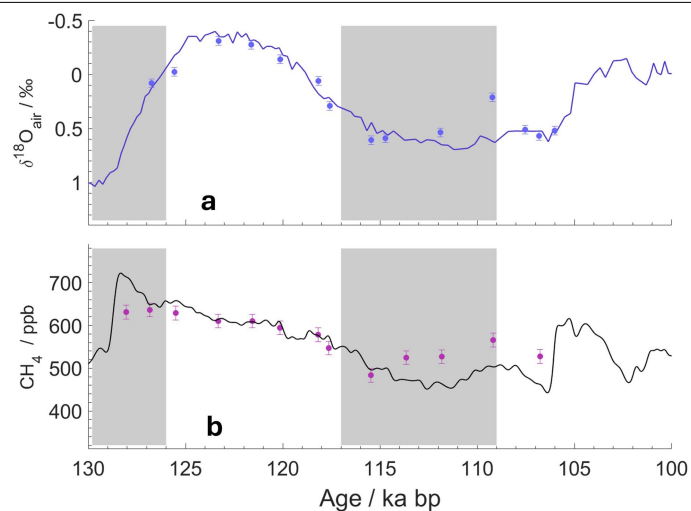
Extended Data Fig. 2 | $\delta^{18}\text{O}$ for the the SIR ice and East Antarctic cores over the last glacial cycle. (a) Reference data for EDC⁶ (red, δD) and EDML⁴⁴ (blue, $\delta^{18}\text{O}$), scaled 8:1, with the horizontal line being an indicative level for the late Holocene. (b) SIR core data, shown only for the sections with reliable dates. The red crosses are discrete measurements, while the blue line is those made from the CFA meltstream. The dashed line is the average of 2-0 ka. All 3 records are synchronised to the AICC2012 age model. Note that the y-scaling is different in the two panels.



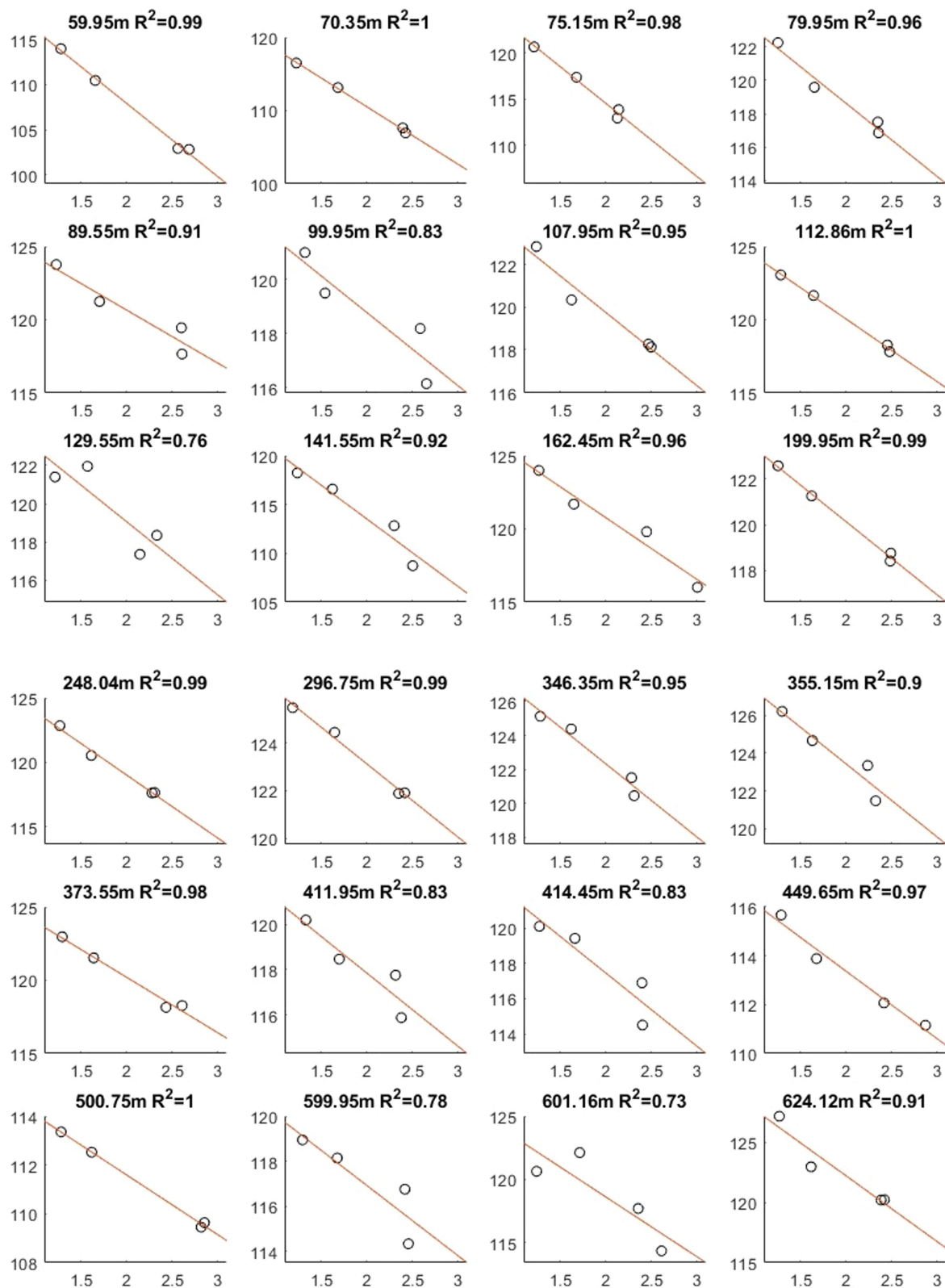
Extended Data Fig. 3 | Total air content data (without cut bubble correction) from SIR. (a) Data for 0-6 ka, (b) for 120-126 ka. Only data with weight ranging between 40 and 80 g are shown, to limit the deviations that would be caused by cut bubbles within each depth span. The blue lines are the SIR averages (2-0.45 ka, 126-120 ka) used in the text.



Extended Data Fig. 4 | A time series of modelled ice sheet and ice shelf extent in the Weddell Sea sector of Antarctica. This is the time series for the model run highlighted in Fig. 4, which shows the 127 ka time slice in more detail. Model output maps were plotted using Generic Mapping Tools v.6.



Extended Data Fig. 5 | SIR CH₄ and δ¹⁸O_{atm} between 100 and 130 ka emphasizing the robust nature of the dating for the LIG section used in this paper. (a) δ¹⁸O_{atm}; discrete measurements from SIR shown as symbols, while the solid line is reference data. (b) Same as (a) but for CH₄. Sections with unreliable ages (605-617 m and >627 m) are greyed out. The error bars are the combined uncertainty (at 1 sigma) of the Skytrain and reference data. Figure reproduced from ref. 35, Copernicus Publications, under a Creative Commons licence CC BY 4.0.



Extended Data Fig. 6 | Plots used to estimate the cut-bubble correction for TAC at different depths. The y-axis is the measured air content (mL kg⁻¹), while the x-axis is S/V (cm⁻¹). See methods for explanation of how these plots were used.

Extended Data Table 1 | Concentrations of ssNa at different times at SIR

Time period ka	ssNa average $\mu\text{g kg}^{-1}$	Indicative distance km
0.1-0 (recent)	65	680 (actual)
7-5	59	700
10-8	26	980
120-118	52.1	740
125-121	41.4	820

Indicative distance is the distance between SIR and the Ronne Ice Shelf edge calculated based on the best fit line of the spatial data³⁷.

Article

Extended Data Table 2 | Differences in measured water isotope ratios between the LIG and the Holocene around Antarctica

	Age model	Mean 0-7.5 ka	Mean 120-126 ka	D or 18O	D diff	O18 diff
Vostok	AICC2012	-440.1	-437.81	D	2.29	0.29
EDC	AICC2012	-396.7	-387.01	D	9.69	1.21
EDML	AICC2012	-44.62	-44.15	18O		0.47
Taldice	AICC2012	-36.35	-36.17	18O		0.18
Dome Fuji	AICC2012	-54.71	-53.73	18O		0.98
Taylor Dome	st9810	-39.74	-38.4	18O		1.34
Average						0.74
Skytrain	ST2022- AICC2012	-30.9	-28.7	18O		2.2

Differences in δD are converted to equivalent differences in $\delta^{18}O$ using a ratio of 8:1. Original isotopic data for Vostok⁶², EDC⁶, EDML⁴⁴, Taldice⁶³, Dome Fuji⁶⁴ and Taylor Dome⁶⁵.